Transition to turbulence via spatiotemporal intermittency in stimulated Raman backscattering

M. M. Škorić,[1] M. S. Jovanović,[2] and M. R. Rajković[1]
[1]*Vinča Institute of Nuclear Sciences, P.O. Box 522, 11001 Belgrade, Yugoslavia*
[2]*Department of Physics, University of Niš, P.O. Box 91, 18001 Niš, Yugoslavia*
(Received 13 April 1995; revised manuscript received 10 October 1995)

The spatiotemporal evolution of stimulated Raman backscattering in a bounded, uniform, weakly dissipative plasma is studied. The nonlinear model of a three-wave interaction involves a quadratic coupling of slowly varying complex amplitudes of the laser pump, the backscattered and the electron plasma wave. The corresponding set of coupled partial differential equations with nonlinear phase detuning that is taken into account is solved numerically in space time with fixed nonzero source boundary conditions. The study of the above open, convective, weakly confined system reveals a quasiperiodic transition to spatiotemporal chaos via spatiotemporal intermittency. In the analysis of transitions a dual scheme borrowed from fields of nonlinear dynamics and statistical physics is applied. An introduction of a nonlinear three-wave interaction to a growing family of paradigmatic equations which exhibit a route to turbulence via spatiotemporal intermittency is outlined in this work.

PACS number(s): 52.35.Ra, 42.65.Dr, 05.45.+b, 52.40.Nk

I. INTRODUCTION

The nonlinear three-wave interaction (3WI) as a physical concept, in its variety of appearances, has found its application in hydrodynamics, nonlinear optics, and plasma physics [1]. It occurs whenever waves encounter a resonance in a physical space, i.e., fulfill frequency and wave vector matching conditions. Stimulated Raman scattering (SRS) in plasma is a paradigm of a three-wave interaction related to a nonlinear coupling of intense laser light (pump) to the electron plasma wave (EPW) and the scattered light, shifted in wave number and frequency [2,3]. It has been studied to a great extent both experimentally and theoretically, largely because of its practical application in a search for a future energy source based on inertial confinement thermonuclear fusion induced by intense laser beams. That is, SRS belongs to a family of underdense plasma instabilities, which can have a detrimental effect on the efficiency of laser energy deposition into a fusion target. The well-developed parametric theory [2,3] gives basic values of SRS instability threshold, growth rates in its initial stage, and some insight into long time spatiotemporal evolution in saturated regimes [2,4–6]. However, in contemporary high-intensity laser-plasma experiments, SRS has often displayed rich and exciting physics, not predicted by the parametric theory, such as a spiky-burstlike signal, anomalously low reflectivity, and spectral gaps and broadenings, as well as incoherent (irreproducible) dynamics [5]. With increasing evidence that SRS often transits from convective to absolute instability in typical laser fusion target-plasma experiments, the problem of nonlinear saturation has become a focus of many SRS studies. Various models, based on different physical mechanisms, have been recently attempted, pointing to a strongly nonlinear dynamics of the EPW as a key factor that determines the nature of saturated SRS states [7]. In particular, an inherent feature of strongly nonlinear SRS to transit from a coherent (regular) to chaotic (turbulent) dynamics has been anticipated recently [5,6,8]. In this paper, transition from a coherent to a strongly nonlinear incoherent regime, or spatiotemporal chaos (STC) [9], is studied for saturated SRS in typical laser fusion conditions. This study follows and extends recent work by the same authors [6,10] on nonlinear saturation of SRS in a plasma layer as a paradigm of a ubiquitous 3WI in a dissipative, weakly confined spatially extended system, which can exhibit extensive chaos [8–10]. The corresponding set of coupled partial differential equations (PDEs), with nonlinear phase detuning of the EPW taken into account, is solved numerically in space time with rigid nonzero source boundary conditions. Through the variation of physical (laser and plasma) parameters, in particular by increasing the pump strength, this open, convective system is driven toward a spatiotemporal chaos. A route via steady state and periodic regime with quasiperiodic transition to spatiotemporal intermittency is observed.

The spatiotemporal intermittency (STI) in which periodic or quasiperiodic, coherent (laminar) oscillations are interrupted by chaotic (turbulent) bursts is a widely observed phenomenon in spatially extended systems [9,11,12] with effectively many degrees of freedom, for example, in hydrodynamic systems (Rayleigh-Bénard convection, surface waves, and open pipe flows [13]). This state should be contrasted with the weak or phase turbulence, where there is a competition between localized coherent structures in the sense that one mode dominates energetically, then another takes over, and so on. These localized structures occur at random within the physical domain, which retains a rather homogeneous structure as, for example, in Rayleigh-Bénard convection, and such dynamics is usually low dimensional. As such, weak turbulence is closest to the so-called low-dimensional chaos in which the system displays incoherence only in time while the spatial structure remains quasifrozen by the confined boundaries [14]. The spa-

tiotemporal intermittency, on the other hand, is further characterized by dominant macroscopic scales in space time, which can, generally taken, be identified as the coherent (length, time) scales in distinction to fully developed turbulence, where there are no predominant macroscopic scales. In addition to experiments in hydrodynamics, the spatiotemporal intermittency is frequently encountered in PDE simulations of routes to chaos generic to nonlinear dissipative extended systems [9,11], modeled by, for example, the Kuramoto-Shivashinsky equation, the Swift-Hohenberg equation, and coupled map lattices [15], to name a few. The STI state displays the coexistence of patches of turbulence immersed in the rest of the structure still in the laminar state; the continuous transition amounts to a progressive increase of the turbulent fraction through the variation of control parameters [11]. In this case turbulence is *strong* locally and affects only a part of a physical space, which can be very small, e.g., at the STI threshold [11]. For completeness, we are reminded that in nonlinear plasma physics an extensively developed theory of weak turbulence is available, starting from the early 1960s. This theory is built on a quasilinear concept of weakly interacting, weakly nonlinear plasma modes of random phases [16].

The rest of the paper is organized as follows. In Sec. II we present the one-dimensional model of the SRS. Then, in Sec. III we use classical diagnostics from dynamical systems theory to analyze the time-only aspect of the backscattered wave. In Sec. IV we address the spatiotemporal aspect of the system and analyze the corresponding patterns and the correlation functions. In Sec. V we introduce dimension and entropy that quantify the spatiotemporal behavior and identify the route to spatiotemporal intermittency and chaos. Finally, in Sec. VI, we coarse grain the degrees of freedom into binary variables such that the local space-time regions are labeled as either chaotic or laminar, and we use techniques from the theory of phase transitions and critical phenomena to identify the transition from spatiotemporal intermittency to spatiotemporal chaos.

II. MODEL EQUATIONS

The one-dimensional model of SRS we are considering assumes a uniform plasma layer of thickness L, irradiated by a laser beam from $x<0$, which enters the plasma at $x\geq 0$. The EPW and the scattered light are allowed to grow from their thermal noise levels (ε_1 and ε_2, respectively). Moreover, the EPW is subjected to a weak dissipation characterized by the linear damping rate ν_e. The nonlinear 3WI model we derive here for the case of SRS describes the spatiotemporal evolution of complex amplitudes of the pump (a_0), scattered (a_1), and EPW (a_2) in a weakly coupling approximation. These equations are obtained from Maxwell's and fluid plasma equations in WKB approximation, assuming the resonant matching between frequencies and wave numbers of three waves ($\omega_0=\omega_1+\omega_2$, $\vec{k}_0=\vec{k}_1+\vec{k}_2$) closely satisfying the linear dispersion relations

$$\omega_{0,1}^2=k_{0,1}^2c^2+\omega_{pe}^2\ ,\quad \omega_2^2=\omega_{pe}^2+3k_2^2v_{Te}^2\ , \tag{1}$$

where indices 0, 1, and 2 stand for the pump, scattered, and EPW, respectively; ω_{pe} for electron plasma frequency; and v_{Te} for electron thermal velocity. For the case of *backscattering,* which is of most practical importance, the corresponding set of 3WI equations reads [6]

$$\begin{aligned}
&\frac{\partial a_0}{\partial\tau}+V_0\frac{\partial a_0}{\partial\xi}=-a_1a_2\ ,\\
&\frac{\partial a_1}{\partial\tau}-V_1\frac{\partial a_1}{\partial\xi}=a_0a_2^*\ ,\\
&\frac{\partial a_2}{\partial\tau}+V_2\frac{\partial a_2}{\partial\xi}+\Gamma a_2=\beta_0^2a_0a_1^*+i\delta|a_2|^2a_2\ ,
\end{aligned} \tag{2}$$

with time and space variables $\tau=\omega_0t$, $\xi=x/L$, where the dimensionless amplitudes of the coupled waves are related to the physical quantities, electric fields E_0 and E_1 of the two electromagnetic waves, and EPW-driven electron density fluctuation δn_e:

$$\begin{aligned}
a_0(\xi,\tau)&=\frac{ck_2}{4\omega_0}\left[\frac{\omega_{pe}}{\omega_1}\right]^{1/2}\frac{E_0(x,t)}{\mathcal{E}_0}\ ,\\
a_1(\xi,\tau)&=\frac{ck_2}{4\omega_1}\left[\frac{\omega_{pe}}{\omega_0}\right]^{1/2}\frac{E_1(x,t)}{\mathcal{E}_0}\ ,\\
a_2(\xi,\tau)&=\frac{\omega_{pe}^2}{4\omega_0\sqrt{\omega_0\omega_1}}\frac{\delta n_e(x,t)}{n_0}\ .
\end{aligned} \tag{3}$$

$\mathcal{E}_0$ denotes the vacuum value of the pump electric field amplitude, and n_0 the equilibrium plasma density.

Normalized group velocities and the damping Γ are expressed by

$$V_0=\frac{c^2k_0}{\omega_0^2L}\ ,\quad V_1=\frac{c^2k_1}{\omega_0\omega_1L}\ ,\quad V_2=\frac{3k_2v_{Te}^2}{\omega_0\omega_{pe}L}\ ,\quad \Gamma=\frac{\nu_e}{2\omega_0}\ ,$$

and the laser pump strength is given by the ratio of the electron quiver velocity in a laser pump field to the speed of light:

$$\beta_0=\frac{v_{\rm osc}}{c}=\frac{eE_0}{m_e\omega_oc}\ .$$

We note an additional self-modal nonlinearity in the equation for EPW, given in the form of a nonlinear phase detuning (shift) $\sim\delta|a_2|^2$, which is due to large amplitude EPWs induced through the SRS process [3,7]. In present-day laser-plasma interaction experiments, high-intensity lasers induce large amplitude EPWs. For short pulse, ultra high intensities, relativistic correction to the electron mass makes it necessary to include a nonlinear detuning term in (2) [17]. On the other hand, a similar term could be due to nonlinear density modulation involving pondermotive coupling of EPWs to ion motion. While relativistic correction to electron plasma frequency directly adiabatically induces nonlinear detuning of the wave resonance, density modulation has a more complex time-dependent effect due to ion dynamics [4]. Therefore, in the latter case, nonlinear equations given by (2) are basically of a model type. For high-intensity laser-

plasma interaction, the corresponding model studied by other authors [17] assumes a relativistic detuning parameter δ, given as

$$\delta=\frac{3\omega_0^2\omega_1}{c^2\omega_{pe}k_2^2} . \tag{4}$$

We also note the relevance of the model (2) to relativistic beat wave interactions [17].

The standard conservative form ($\delta=0$, $\Gamma=0$) of 3WI in one dimension is integrable [1]. However, with an introduction of dissipation ($\Gamma>0$), closed form solutions exist no longer. A spatially uniform (time-only) version of (2) has been studied in detail, and it was shown to exhibit a low-dimensional chaos under restricted conditions [18]. A spatially extended model of 3WI is more difficult to investigate. Only recently, the 3WI was solved and studied in space time. These results have revealed rich physical behavior of saturated regimes corresponding to low-dimensional chaos as well as to STC [6,8].

The most useful information on the SRS is contained in the reflectivity R, which designates a fraction of incident laser intensity reflected backward,

$$R=\frac{V_0|a_1(0)|^2}{V_1|a_0(0)|^2} ,$$

with its maximum normalized to unity in the stationary case. To solve (2), appropriate initial and boundary conditions are required. We choose physically relativistic boundary conditions, while the choice of the plasma slab length satisfies the criterion for the occurrence of the absolute instability. The wave amplitudes obey the corresponding initial and nonzero source fixed boundary conditions,

$$a_0(x,0)=0 \quad (\text{for } x>0) , \quad a_0(0,t)=A_0$$

$$a_1(x,0)=a_1(L,t)=\varepsilon_1 A_0 , \quad a_2(x,0)=a_2(0,t)=\varepsilon_2 ,$$

where A_0 follows from (3) for $E_0(0)=\mathcal{E}_0$.

A series of numerical simulations of our model (2), by means of a central difference method, has been performed for different system (laser and plasma) parameters within physically realistic values. The accuracy of the centered-time, centered-space numerical scheme has been checked at each temporal step by using the modified Manley-Rowe conservation relations [2], which follow from (2). We focus on the following parameter values: $V_0=9.5\times10^{-3}$, $V_1=8.8\times10^{-3}$, $V_2=2.9\times10^{-4}$, $\Gamma=1.6\times10^{-6}$, $\delta=3.5$, $\varepsilon_1=0.01$, $\varepsilon_2=0$, corresponding to a set of typical laser plasma conditions [4]: $n_0=0.1n_{cr}$, $T_e=1$ keV, $L=100\,c/\omega_0$, and $\nu_e/\omega_{pe}=10^{-5}$.

III. BIFURCATION SEQUENCE AND LOW-DIMENSIONAL CHAOS

In the time-only aspect of the SRS we follow the evolution of the backscattered wave. For the present exposition we study the bifurcation sequence while the incident wave amplitude, as a control parameter, is varied. The justification for this choice of the control parameter lies in the fact that the variation of the plasma slab length, keeping the incident laser beam amplitude fixed, leads to the same bifurcation sequence. The variation of the damping term, on the other hand, alters only the quasiperiodic regime, as discussed below, and the same effect is observed when plasma density is changed. We have verified the robustness of the scenario by varying the plasma slab length up to a factor of 5, changing the damping term by two orders of magnitude ($10^{-6}-10^{-4}$)ν_e/ω_p, and varying the plasma density within the interval ($0.001n_{cr}$-$0.1n_{cr}$).

As the relative pump strength β_0 increases, starting from the value 0.01, the attractor changes according to the symbolic sequence

$$\text{FP}\rightarrow\text{P}\rightarrow\text{QP}\rightarrow\text{I}\rightarrow\text{C}$$

where FP stands for unimodal fixed point, P for periodic, QP for quasiperiodic, I for intermittent, and C for chaos. The quantitative boundaries in β_0 between successive attractors are depicted in Fig. 1. The fixed point bifurcates to a stable limit cycle [Fig. 2(c)] through a supercritical Hopf bifurcation. As the relative pump strength is further increased, an additional spatial mode occurs, which is apparently associated with the second frequency in the quasiperiodic dynamics observed in the interval ($0.026\leq\beta_0\geq0.029$). The corresponding second frequency occurring for the EPW can be accounted for by the appearance of a traveling wave [Fig. 8(b)]. Within this finite parameter range, a mode locking occurs in which two incommensurate frequencies become related by a ratio of integers and the winding number, defined as the ratio of the two frequencies, is equal to 5. The corresponding phase space representation, a 2-torus, is represented in Fig. 3(c). Harmonics f_n, appearing in the power spectrum of the quasiperiodic dynamics, are related to the two main frequencies by $f_n-f_0=n(f_1-f_0)$, where f_0 is the frequency of the peak to the left of the most energetic frequency f_1 [Fig. 3(b)]. The weak nonlinear effects stabilize the 2-torus trajectory in the vicinity of the former periodic trajectory, which although linearly unstable remains visible, disclosing a beautiful illustration of another supercritical Hopf bifurcation. At this point, it should be noted that the increase of the damping term leads to the bifurcation sequence in which the quasiperiodic regime occurs without frequency locking, which can be explained on the basis that increased damping suppresses the evolution of the traveling mode. With further increase in β_0, the manifestation of another degree of freedom occurs through the destruction of torus without appearance of the third frequency [Figs. 4(b) and 4(c)]. An interesting feature of this new regime is the existence

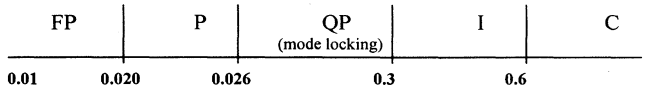

FIG. 1. The bifurcation sequence as a function of relative pump strength.

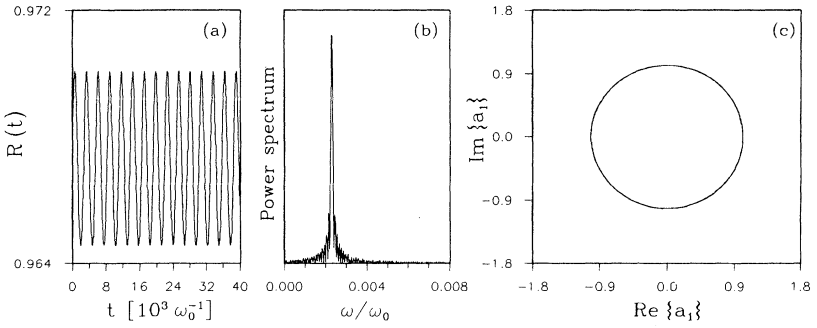

FIG. 2. (a) Stimulated Raman backscattering reflectivity, (b) power spectrum, and (c) phase diagram for $\beta_0=0.025\,34$.

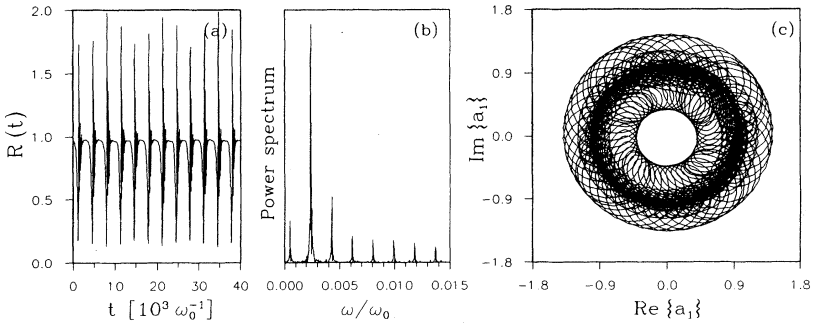

FIG. 3. (a) Reflectivity, (b) power spectrum, and (c) phase diagram, for $\beta_0=0.027$.

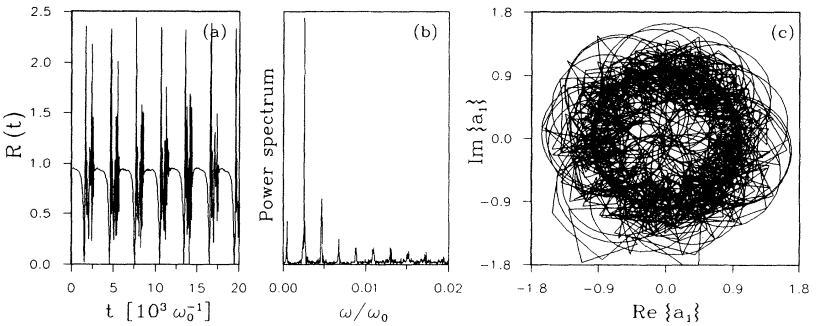

FIG. 4. (a) Reflectivity, (b) power spectrum, and (c) phase diagram for $\beta_0=0.03$.

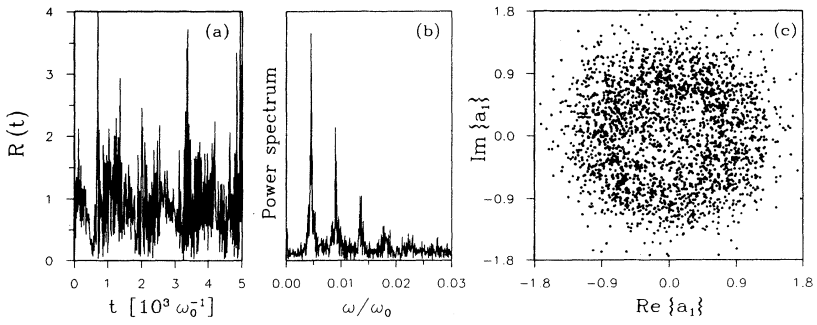

FIG. 5. (a) Reflectively, (b) power spectrum, and (c) phase diagram for $\beta_0=0.05$.

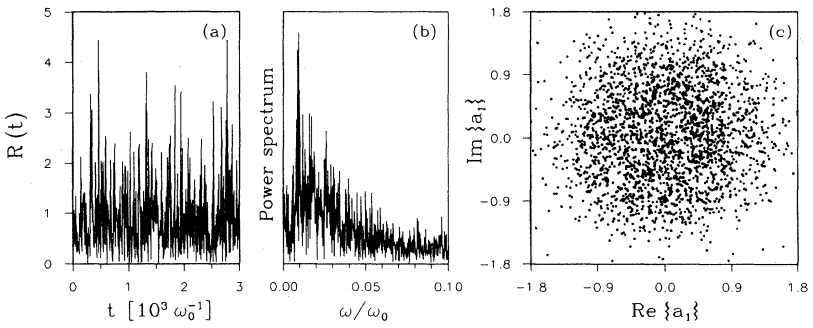

FIG. 6. (a) Reflectivity, (b) power spectrum, and (c) phase diagram for $\beta_0=0.1$.

of two metastable regions of the attractor, namely, "laminar" parts that retain almost unchanged a quasiperiodic nature and intermittent chaotic bursts. In the power spectra plots, the power spectrum of intermittent regime exhibits an increasing noise level [Figs. 4(b) and 5(b)]. As the control parameter is further increased, the fraction of time spent in laminar regions decreases, and fully developed temporal chaos sets in, as reflected in the broadband power spectrum [Fig. 6(b)].

Finally, the correlation dimension values obtained by the standard Grassberger-Procaccia algorithm [19] establish the low-dimensional nature of these attractors. The dimension increases from 1 (periodic) through 2.28 (quasiperiodic) to 3.7–4.7 (intermittent and chaotic).

All of the dynamical system diagnostics presented in this section analyzed the temporal aspect of the backscattered wave at the left boundary of the plasma slab. For a system of partial differential equations (1), the temporal aspects must be correlated with spatial information, and more detailed insight is gained from the analysis of spatiotemporal patterns and the corresponding correlation functions. This is the subject of the next section.

IV. SPATIOTEMPORAL PATTERNS

The simulation results of the stimulated Raman backscattering dynamics exhibit spatiotemporal intermittency and spatiotemporal chaos and are described in terms of correlation functions having spatial and temporal scales. The numerically observed spatial states involved in the bifurcation sequence include coherent states, traveling waves, and intermittent and chaotic states. The global picture of both spatial and temporal attracting states for various spatiotemporal regimes for the backscattered wave and the EPW are listed in Table I. In general, the qualitative space-time behavior of the pump wave is al-

TABLE I. Main features of spatial and temporal patterns for the backscattered wave (BSW) and the electron plasma wave (EPW).

Regime	Spatial structure		Temporal response	
	BSW	EPW	BSW	EPW
I $0.01 \le \beta_0 < 0.025$	Semihumplike structure	Semihumplike structure	Steady state	Steady state
II $0.025 \le \beta_0 < 0.026$	Periodic structure superimposed on humplike underlying structure	Semihumplike structure	Single periodic	Single periodic
III $0.026 \le \beta_0 < 0.03$	One localized breatherlike structure superimposed on hump	Traveling wave	Quasiperiodic; mode locking	Quasiperiodic; mode locking
IV $0.03 \le \beta_0 < 0.04$	One localized breatherlike structure with several smaller, irregularly shaped structures superimposed on humplike structure	Damped traveling wave; ridgelike structures at right end	Intermittent; quasiperiodic nature of laminar parts	Intermittent; quasiperiodic nature of laminar parts
V $0.04 \le \beta_0 < 0.06$	Chaotic, with intermittent laminar region	Damped traveling wave; ridgelike structures interrupted by laminar domains	Intermittent	Intermittent; chaotic
VI $\beta_0 \ge 0.06$	Chaotic	Chaotic	Chaotic	Chaotic

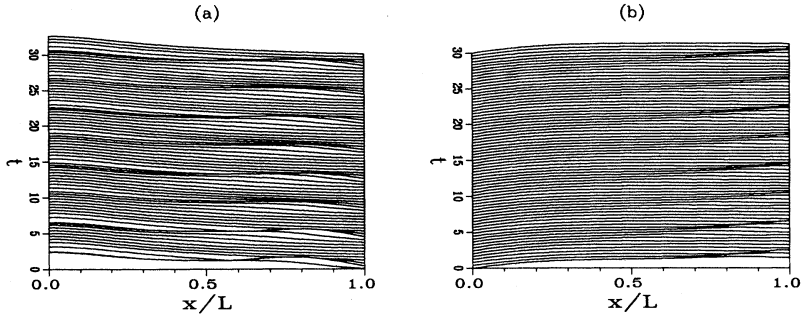

FIG. 7. Space-time patterns of (a) the backscattered wave and (b) the electron plasma wave for $\beta_0=0.025\,34$.

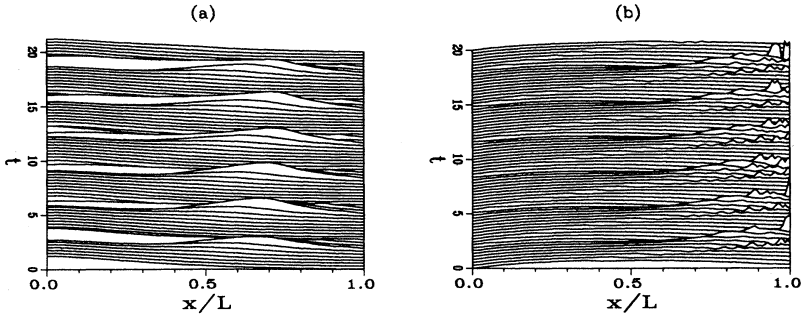

FIG. 8. Space-time patterns of (a) the backscattered wave and (b) the electron plasma wave for $\beta_0=0.027$.

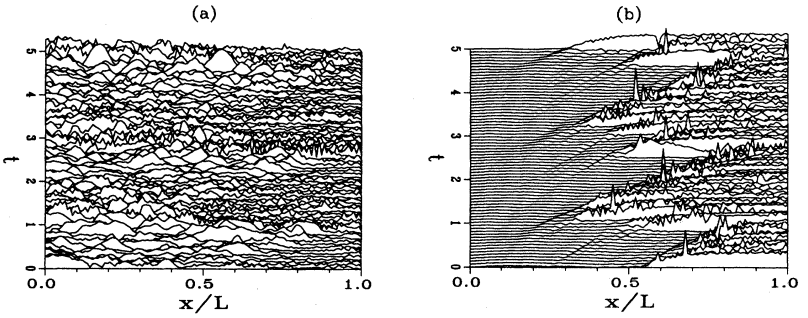

FIG. 9. Space-time patterns of (a) the backscattered wave and (b) the electron plasma wave for $\beta_0=0.06$.

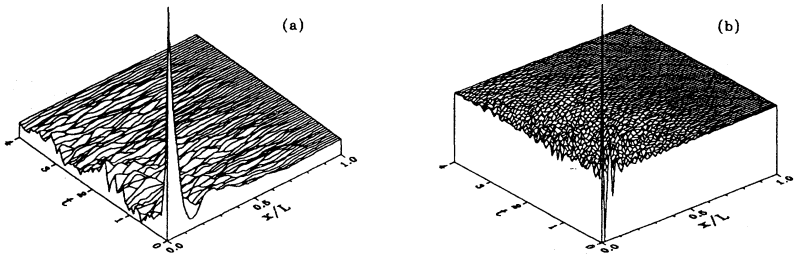

FIG. 10. Autocorrelation functions for (a) the backscattered and (b) the electron plasma wave for $\beta_0=0.06$.

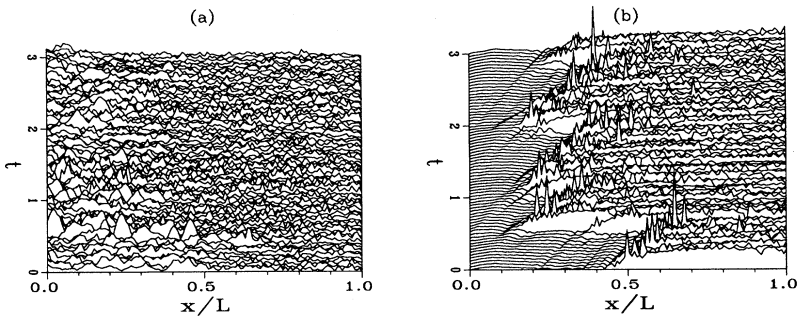

FIG. 11. Space time patterns of (a) the backscattered wave and (b) the electron plasma wave for $\beta_0=0.1$.

most identical to the corresponding patterns of the scattered wave. This is due to the fact that the coherent structures of the backscattered wave are determined by the incident pump wave, while the features of the EPW represent the outcomes of the interaction processes that take place between the pump and the backscattered wave. We give here a more detailed account of these spatiotemporal structures. For small values of the relative pump strength (regime I of Table I), the spatial structure resembles a semi-humplike structure that increases in size as the damping term (Γ) decreases. The mirrorlike symmetry of the scattered wave structure and the EPW structure with respect to each other is evident in Fig. 7. In regime II of Table I, a spatially periodic structure of the scattered wave superimposed on one-half of the hump occurs at regular time intervals, while no such structure can be noticed for the EPW. Further increase of the control parameter β_0 (regime III) brings forth the appearance of the propagating EPW mode and flattening of the underlying spatial structure for both waves. The striking feature of the scattered wave pattern in this regime is the breatherlike coherent excitation oscillating in time [Fig. 8(a)]. As β_0 increases and leaves the parameter range corresponding to the mode locking temporal behavior, the most interesting feature is the change in spatial symmetry, particularly for the EPW. As the relative pump strength increases to regime IV, the temporal translational symmetry of the backscattered coherent structures breaks up more dramatically than the corresponding one of the EPW. A common feature of all four regimes is the same number of coherent structures in the time direction.

The transition from the spatiotemporal intermittency (regime V, Fig. 9) to spatiotemporal chaos (regime VI, Fig. 11) is continuous in the sense that, as the threshold is approached from below, the number of turbulent domains slowly increases, accompanied with the breakup of laminar domain fronts. The autocorrelation functions for the two regimes (Figs. 9, 10, and 12) clearly show that the correlations fall off gradually both in time and in space. The well-defined correlation lengths (times) for these two regimes indicate that the dynamics is uncorrelated for lengths (times) greater than these characteristic values. The fact that the group velocity of the EPW is 30 times smaller than the backscattered wave velocity has important complications on the spatiotemporal characteristics of the corresponding wave patterns. The correlation length of the EPW is consequently approximately 30 times smaller than the correlation length of the backscattered wave (Figs. 10–12). Autocorrelation functions for regimes V and VI provide clear qualitative, although quantitatively not adequate, evidence of spatiotemporal chaos. Moreover, to determine the control parameter value at which the transition from intermittency to chaos occurs, methods from the theory of critical phenomena and phase transitions will be used. These aspects of the analysis are addressed in the next two sections.

V. QUANTITATIVE SIGNATURES OF SPATIOTEMPORAL REGIMES

To understand the transition from regular to chaotic dynamics, the relationship between the spatial and temporal degrees of freedom in the system is essential. In this study we choose the local approach on the attractor of the EPW in order to define the spatiotemporal quantities such as dimension and entropy. The approach is characterized by determination of *local* orthogonal directions on the attractor (the local topological dimensionali-

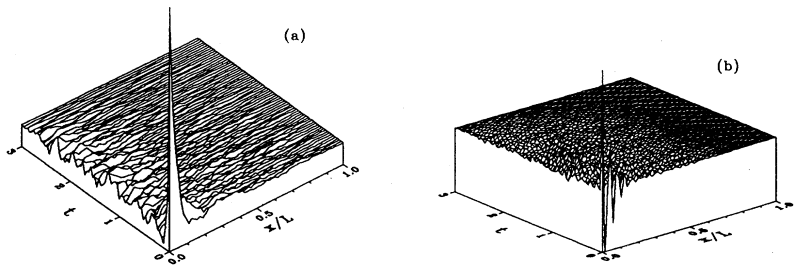

FIG. 12. Autocorrelation functions for (a) the backscattered wave and (b) the electron plasma wave for $\beta_0=0.1$.

ty) along which the local data points are distributed. The embedding space, and hence the attractor, is reconstructed with reference to spatial dependence. That is, embedding procedure consists in taking time series of each spatial location as one component of the embedding vector, and the number of spatial locations determines the embedding dimension. The centers defining local regions on the attractor are randomly selected in such a way that they nearly cover the entire surface of the attractor. The local dimension is determined by the rank of the local data matrix defined by the preselected number of nearest neighbors for each local center. The number of nearest neighbors is determined by the condition that the local region they define is linear and their number usually varies between 30 and 50. The test for local linearity consists in successively decreasing the number of points in the local region until further decrease does not decrease the number of dominant orthogonal directions [20]. The rank of the local data matrix is determined by the singular value decomposition (SVD). If the local data matrix is labeled $\mathbf{U}$, then the singular values λ_i of $\mathbf{U}$ are equal to the square roots of the eigenvalues of the data covariance matrix $\mathbf{R}=\mathbf{U}^T\mathbf{U}$, and the number of nonzero singular values (eigenvalues) determines the local topological dimension of the attractor. Since it is almost impossible to obtain exactly zero eigenvalues either in numerical simulations or from experimental data, the main challenge in this approach is to determine the threshold below which an eigenvalue should be considered to be zero. The topological dimension of the whole attractor is calculated as the weighted average of local dimensions, i.e.,

$$\langle D \rangle = n_1 d_1 + n_2 d_2 + \cdots + n_s d_s \ ,$$

where $n_i = m_i / N$, m_i is the number of local regions in which dimension d_i occurs, and N is the total number of local regions. Hence, as the local dimension is an integer value, the topological dimension of the whole attractor may be fractal in nature. Note that because of the nature of the embedding procedure, the dimension defined in such a way reflects the spatial and temporal dynamics simultaneously.

The separation of true signal from noise is accomplished using the method formulated on the basis of an information-theoretic criterion. Two such methods, the Akaike information criterion [21] and the minimum descriptive length of Risannen [22], have been extensively used in signal processing applications, particularly for the determination of the number of signals in high resolution arrays. However, since the Akaike information criterion tends to overestimate and the minimum descriptive length tends to underestimate the number of signal sources, active research is going on to overcome the shortcomings of the these two criteria. In our approach we have used the modified information-theoretic criterion, which does not show these deficiencies, and an interested reader can find a complete account of this method in Ref. [23]. The resulting topological dimensions for various spatiotemporal patterns of the SRS are presented in Fig. 13. As more and more active modes take part in the dynamics, the dimension correspondingly

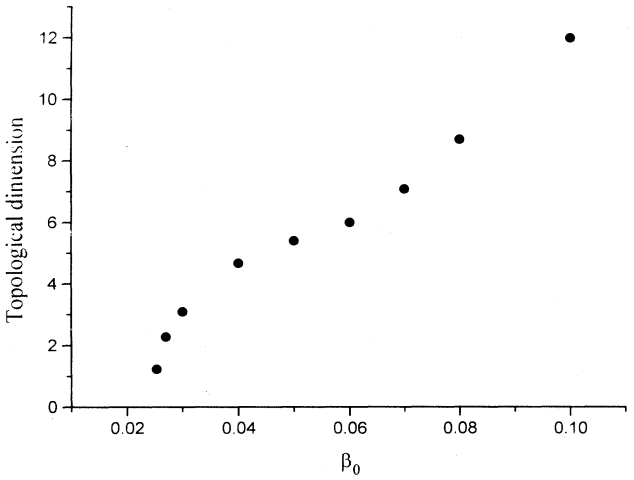

FIG. 13. Topological dimension of the electron plasma wave attractor for various values of the relative pump strength β_0.

changes and various spatiotemporal bifurcations may be identified through the dimension changes. Another important aspect of dimension calculations for extended systems, namely, density of dimension $\rho \equiv D(L)/L$, where L is the size of the system, has been verified as independent of L, and details of the growth rate of dimension as a function of the system size have been reported elsewhere [24].

Using the same embedding procedure, we have applied the Grassberger-Procaccia algorithm for calculating the widely used correlation dimension. The obtained results show very good agreement with the results for topological dimension for low-dimensional dynamics ($d < 8$). For higher dimensional dynamics the correlation dimension is inaccurate because of the intrinsic limitations of the algorithm. That is, the upper bound permitted by the algorithm is $2 \log_{10} N$, where N is the time dimension of the embedding matrix (length of the time series) [25]. In general, however, the advantages of local analysis of topological properties of the attractor are particularly evident in identifying important topological features due to, for example, thin directions, which may indicate that the corresponding attractor cross section is a Canto set, or the effects due to the limited amount of data [26]. Moreover, the criterion for separating signals from noise is the integral part of this approach, while the correlation dimension, as well as other metric and probabilistic dimensions, are quite sensitive to the presence of noise. Note that SVD is often used as a noise reduction procedure before applying the correlation dimension algorithm. That is, the few dominant eigenvalues in the singular value spectrum are retained based on the certain arbitrary criterion, such as by counting those singular values (eigenvalues) that exceed a certain percentage of the largest singular value (eigenvalue), usually $\geq 95\%$ [27]. In either case, SVD is applied globally, while the information is lost on the local effects on noise, which can be of significant im-

portance for thin directions on the attractor.

Important indicators of the sensitivity to initial conditions of the system are Lyapunov exponents, which represent the growth rates of edges of an infinitesimal tangent space to the trajectory of an attractor. In terms of singular values λ_i, the local Lyapunov exponents scale approximately as $\ln\lambda_i$. Hence, the number of local Lyapunov exponents is equal to the local topological dimension, and the number of positive local Lyapunov exponents averaged over the attractor increases with the increase of the control parameter, as well as with the system size.

The singular value decomposition of the spatiotemporal data matrix corresponds to the spectral decomposition of the signal into spatial and temporal orthogonal modes,

$$u(x,t)=\sum_{i=1}^{N}\lambda_i\phi_i(x)\psi_i(t)$$

with

$$\lambda_i\geq\lambda_2\geq\cdots>0$$

and

$$(\phi_i,\phi_j)=(\psi_i,\psi_j)=\delta_{i,j}\ ,$$

which converges in norm. The pair (ϕ_i,ψ_j) defines a spatiotemporal structure of energy λ_i^2 [28]. The relative energy of each structure is given as the ratio of one structure energy to the total energy of the signal [28,29]

$$p_i=\frac{\lambda_i^2}{\sum_{i=1}^{N}\lambda_i^2}\ .$$

Here the characterization of the eigenvalue spectrum is based on the principle that the information contained in the eigenvalues can be interpreted as a probability distribution, so that each eigenvalue can be viewed as an indication of how likely it is to identify a spatiotemporal structure within the whole spectrum. Based on the information-theoretic definition of entropy, the normalized entropy can be defined as

$$H(u)=-\lim_{k\to\infty}\frac{1}{\ln k}\sum_{i=1}^{k}p_i\ln p_i\ .$$

Because of the normalizing factor $1/\log k$, the entropy is defined in the range between 0 and 1. If the dynamics of the system is such that only one eigenvalue is different from zero (i.e., the energy is concentrated in only one eigenvalue), the spatiotemporal entropy is equal to 0, indicating the lowest level of complexity. On the other hand, if the energy is equidistributed, i.e., all eigenvalues are the same, the global entropy is equal to 1, indicating the highest possible complexity. In analogy with the local topological dimension, we can calculate local entropy while the global entropy can be obtained by ensemble averaging over the attractor. The spatiotemporal entropy of the EPW as a function of relative pump strength is presented in Fig. 14. The entropy evolves from a value close to zero corresponding to the steady (laminar) state; increases as new coherent structure emerge and the energy spreads

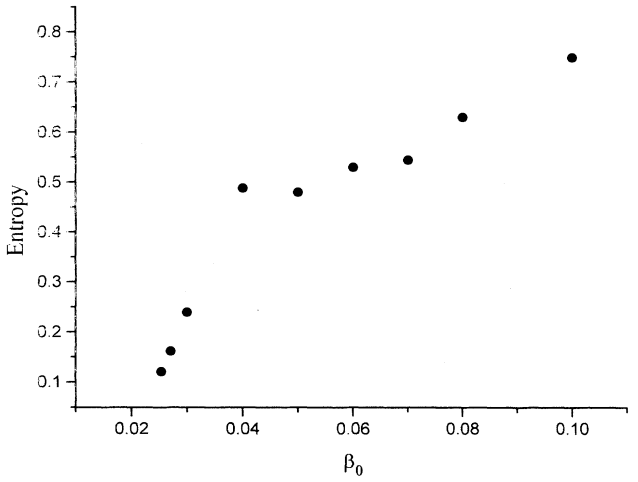

FIG. 14. Entropy of the electron plasma wave for various values of the relative pump strength β_0.

out on the eigenvalues; and approaches the value of 0.76, where many structures carry similar amounts of energy. Both the entropy and the topological dimension display a clear distinction between STI and STC, and work is in progress to relate the local aspects of these two quantities to the universal characteristics of spatiotemporal intermittency and chaos in various physical systems.

VI. TRANSITION FROM SPATIOTEMPORAL INTERMITTENCY TO SPATIOTEMPORAL CHAOS

A method to locate a parameter threshold value is based on the coarse graining of the space-time data into binary values, according to which local spatiotemporal regions are labeled only as either laminar or chaotic

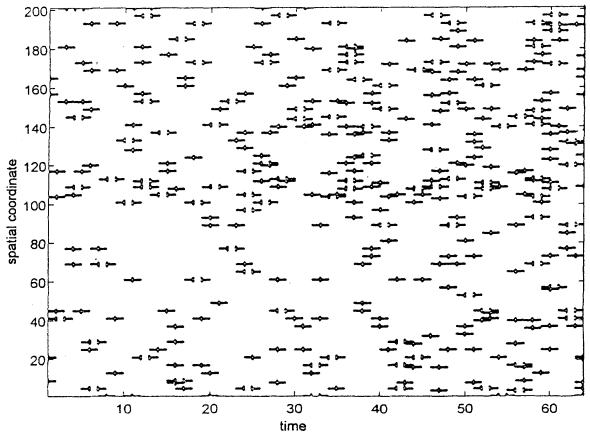

FIG. 15. Spatiotemporal pattern for $\beta_0=0.06$ (near intermittency threshold) following the binary reduction of the space-time data.

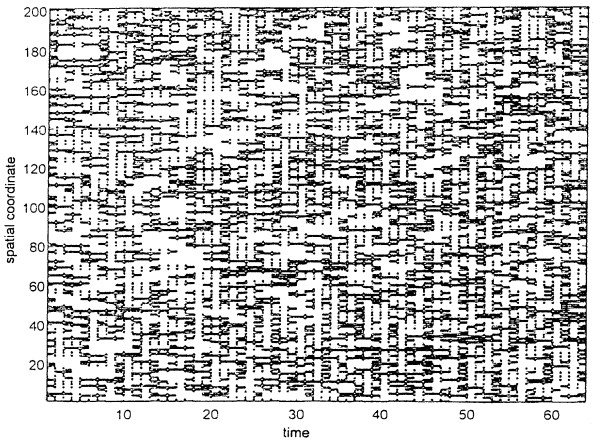

FIG. 16. Spatiotemporal pattern for $\beta_0=0.1$ (well in the turbulent region) following the binary reduction of the space-time data.

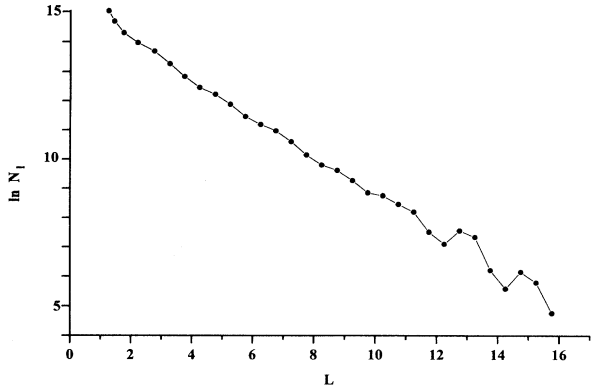

FIG. 18. Histogram of the sizes of laminar domains for $\beta_0=0.1$ (well in the turbulent region); semilogarithmic plot reveals exponential decay with a characteristic exponent 0.65.

[30,31]. Since in the laminar (quasiperiodic) regions the local amplitude is lower than in turbulent regions, by setting an arbitrary cutoff a binary representation may be obtained that easily distinguishes between chaotic and nonchaotic domains. The obtained representation seems to be independent on the precise cutoff value within the accuracy of the calculation. The two-state representation for the regimes corresponding to $\beta_0=0.06$ and $\beta_0=0.1$ are presented in Figs. 14 and 15, respectively. Assuming an analogy to directed percolation [32], the laminar phase corresponds to a state where chaotic (turbulent) states percolate through the lattice until the size in the time direction, the time-correlation length, is reached. Directed percolation is known for exhibiting a continuous (second order) phase transition, usually characterized by a critical exponent that scales the variation of the order parameter near the transition point. The order parameter in this framework is defined as the mean number of laminar or turbulent domains. The distribution of sizes of laminar domains, or the corresponding distribution of sizes of clusters of laminar sites, defines a correlation length (or size) that characterizes the patterns; Figs. 16–18 clearly confirm the existence of a critical threshold

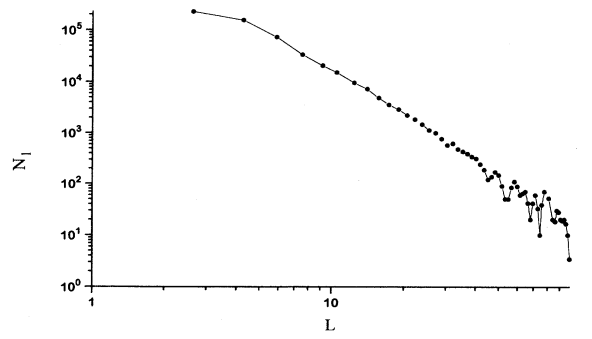

FIG. 17. Histogram of the sizes of laminar domains for $\beta_0=0.06$ (near threshold) displays algebraic decay with exponent 3.0.

value. Near the threshold ($\beta_0=0.06$), the distribution of sizes of laminar domains is characterized by the power law behavior (with the characteristic exponent of the order of 3.0), while deep in the chaotic region ($\beta_0=0.1$) the behavior follows the exponential behavior with the characteristic exponent 1.5. An analogous statistical analysis was performed for the time domain distributions, and the temporal approach displays features similar to those obtained for the spatial distributions. The threshold in this case remains approximately the same ($\beta_0\approx0.06$), although the exponents are different. The distribution follows an algebraic decay, with a characteristic exponent 3.2, while above the threshold the decay is exponential with the characteristic exponent 1.2.

VII. CONCLUSIONS

We have presented a study of the open, convective, weakly confined dissipative model of SRS as a paradigm of 3WI in an extended system. The numerical simulation reveals a particularly beautiful example of a quasiperiodic route, accompanied by frequency locking, to spatiotemporal chaos via spatiotemporal intermittency. The striking feature of this scenario is intermittency in both space and time scales, with laminar regions exhibiting the quasiperiodic nature of the preceding attracting state, as distinguished from the chaotic domains by the change in spatial symmetry. The occurrence of the second frequency in the power spectrum of the quasiperiodic regime is apparently due to the appearance of a new spatial mode in the case of the backscattered wave (traveling wave in the case of the electron plasma wave), suggesting a complex interplay between spatial and temporal degrees of freedom. Changes in the topological dimension of the chaotic attractor can be directly correlated with changes in the number of active modes, and a similar conclusion is valid for the spatiotemporal entropy. An important item of information provided by this analysis is that it supports the view that the route to low-dimensional chaos represents the main dynamical frame on which the route to spatiotemporal chaos is built. The coarse grain-

ing of the space-time data into binary variables enables the use of the methods from the theory of critical phenomena to draw qualitative parallels between the transition from spatiotemporal intermittency to spatiotemporal chaos and directed percolation. The final section of this paper establishes the place of 3WI in the growing family of physical phenomena that display the intermittent route to spatiotemporal chaos.

[1] D. J. Kaup, A. Reiman, and A. Bers, Rev. Mod. Phys. **51**, 915 (1979).

[2] D. W. Forslund, J. M. Kindel, and E. L. Lindman, Phys. Fluids **18**, 1002 (1975).

[3] W. L. Kruer, *Physics of Laser Interactions* (Addison-Wesley, New York, 1988).

[4] J. A. Heikkinen and S. J. Karttunen, Phys. Fluids **29**, 1291 (1986); G. Bonnaud, D. Pesme, and R. Pellat, Phys. Fluids B **2**, 1618 (1990); T. Kolber, W. Rozmus, and V. T. Tikhonchuk, *ibid.* **5**, 138 (1993), and references therein.

[5] H. P. Drake and S. H. Batha, in *Nonlinear and Chaotic Phenomena in Plasmas, Solids and Fluids,* edited by W. Rozmus and J. A. Tuszynski (World Scientific, Singapore, 1991), p. 345.

[6] M. M. Škorić and M. S. Jovanović, in *Laser Interaction and Related Plasma Phenomena,* edited by G. H. Miley and H. Hora (AIP, New York, 1994), Vol. 11, pp. 380–389.

[7] W. L. Kruer, Phys. Scr. **T30**, 5 (1990); F. Chen, *ibid.* **T30**, 14 (1990); R. Bingham, *ibid.* **T30**, 24 (1990); W. Rozmus, *ibid.* **T30**, 64 (1990).

[8] C. C. Chow, A. Bers, and A. K. Ram, Phys. Rev. Lett. **68**, 3379 (1992).

[9] M. C. Cross and P. Hohenberg, Rev. Mod. Phys. **65**, 851 (1993).

[10] M. S. Jovanović and M. M. Škorić, in Physics of Ionized Gases, edited by M. Milosavljević (NOVA Science, New York, in press).

[11] P. Manneville, *Dissipative Structures and Weak Turbulence* (Academic, San Diego, 1990).

[12] D. Stassinopoulos and P. Alstrøm, Phys. Rev. A **45**, 675 (1992).

[13] R. Ramshankar and K. R. Sreenivasan, Physica **23D**, 246 (1986).

[14] Aceves, H. Adachihara, C. Jones, J. C. Lerman, D. W. McLaughlin, J. V. Moloney, and A. C. Newell, Physica **18D**, 85 (1986).

[15] K. Kaneko, Prog. Theory. Phys. **74**, 1033 (1985).

[16] R. Z. Sagdeev and A. Galeev, *Nonlinear Plasma Theory* (Benjamin, New York, 1969).

[17] M. N. Rosenbluth and C. S. Liu, Phys. Rev. Lett. **29**, 701 (1972); C. J. McKinstrie and D. F. Dubois, Phys. Fluids **31**, 278 (1988); T. W. Johnston, P. Bertrand, A. Ghizzo, M. Shoucri, E. Fijalkow, and M. R. Feix, Phys. Fluids B **4**, 2523 (1992), and references therein.

[18] C. Meunier, M. N. Bussac, and G. Laval, Physica **4D**, 236 (1982).

[19] P. Grassberger and I. Procaccia, Physica **9D**, 189 (1983).

[20] K. Fukunaga and R. R. Olsen, IEEE Trans. Comput. **20**, 176 (1971).

[21] H. Akaike, IEEE Trans. Autom. Control **19**, 716 (1974).

[22] J. Rissanen, Automatika **14**, 465 (1978).

[23] K. M. Wong, Q. T. Zhang, J. P. Reilley, and P. C. Yip, IEEE Trans. Acoust. Speech Signal Process. **38**, 11 (1990).

[24] M. M. Škorić, M. S. Jovanović, and M. R. Rajković, in *Dynamical Systems and Chaos,* edited by Y. Aizawa, S. Saito, and K. Shiraiwa (World Scientific, Singapore, 1995), pp. 165–176.

[25] D. Ruelle, Proc. R. Soc. London, Ser. A **427**, 241 (1990).

[26] A. Passamante, T. Heideger, and M. Gollub, Phys. Rev. A **39**, 3640 (1989).

[27] L. Sirovich, Q. Appl. Math **45**, 561 (1987).

[28] N. Aubry, R. Guyonnet, and R. Lima, J. Stat. Phys. **64**, 683 (1991).

[29] M. Rajković, J. Riznić, and M. Ishii, Nucl. Eng. Des. **149**, 53 (1994).

[30] H. Chaté and P. Manneville, Phys. Rev. Lett. **58**, 112 (1987).

[31] P. C. Hohenberg and B. I. Shraiman, Physica **37D**, 109 (1993).

[32] Y. Pomeau, Physica **23D**, 3 (1986).